

ANOMALOUSLY DEEP EARTHQUAKES BENEATH THE NEW HEBRIDES TRENCH

BY S. W. ROECKER, J.-L. CHATELAIN, B. L. ISACKS, AND R. PREVOT

ABSTRACT

The central New Hebrides island arc is a morphologically complex area where the island blocks of Santo and Malekula replace the trench and override the D'Entrecasteaux Fracture Zone (DFZ), a major aseismic ridge, on the subducting plate. Earthquakes recorded by a local network have been located beneath the trench southwest of Malekula at depths of 60 to 90 km. Because these locations are unusual, and because tests with hypothetical data showed that two minima, one for shallow depths and one for deep depths, exist on the travel-time surface for events in this area, we investigated these hypocenters in more detail. Location quality was judged primarily by the fit to *P* and *S* wave arrival times calculated in a variety of velocity models. We found that while the standard deviations of the travel time residuals from some of the events were nearly the same for shallow and deep locations, they were significantly lower for several events at the deeper minimum. Moreover, the marginal *a posteriori* density functions for depth indicate that the deeper depths are significantly more probable. Activity in this area appears to be sporadic. Most of the events were aftershocks of a large earthquake ($M_w = 7.1$) in 1981, and a cluster of events was reported to have occurred in the same area over a period of one month in 1986. The existence of deep earthquakes in this area may be due to interactions of the DFZ with Santo and Malekula, because their locations follow a trend in the seismicity that parallels the western coast of the island blocks. They also occur directly north of a sharp bend in the trench and near a major seismic discontinuity, and may be a manifestation of recent, en-echelon subduction. If these earthquakes are not occurring along the boundary of a new subduction zone, the inferred existence of brittle failure at depths usually associated with a ductile rheology brings into question our understanding of the mechanics of the oceanic lithosphere.

INTRODUCTION

The New Hebrides arc is part of a larger island arc system that forms the boundary between the subducting Indo-Australian plate and the overriding Pacific plate (Figure 1). Convergence between the two plates occurs here at a rate of about 11 cm/yr and in a direction approximately normal to the trench (Dubois *et al.*, 1977). The present New Hebrides arc has been a region of active subduction for probably less than 6 to 8 MY, having inherited this role when an ancestral Solomons-New Hebrides-Fiji-Tonga subduction zone was disrupted in the late Miocene (Karig and Mammerickx, 1972). The arc appears simple on a large scale, being nearly linear along its 1200 km length from the Santa Cruz islands to the Hunter fracture zone. The upper plate is morphologically complex, however, with the most striking structural anomalies occurring in the central part of the arc between 14°–18°S. In this area, the normal trench, island arc, and back arc rift systems that occur elsewhere along the upper plate are replaced, respectively, by the western island blocks of Santo and Malekula, the central Aoba basin, and the horst-like structures beneath the eastern islands of Maewo and Pentecost. Directly to the west of these structures, on the subducting plate, is a broad, east-west oriented topographic high known as the D'Entrecasteaux "Fracture Zone" (Mammerickx *et al.* 1973; Daniel *et al.*, 1977; Maillet *et al.*, 1982; hereafter referred to as the DFZ).

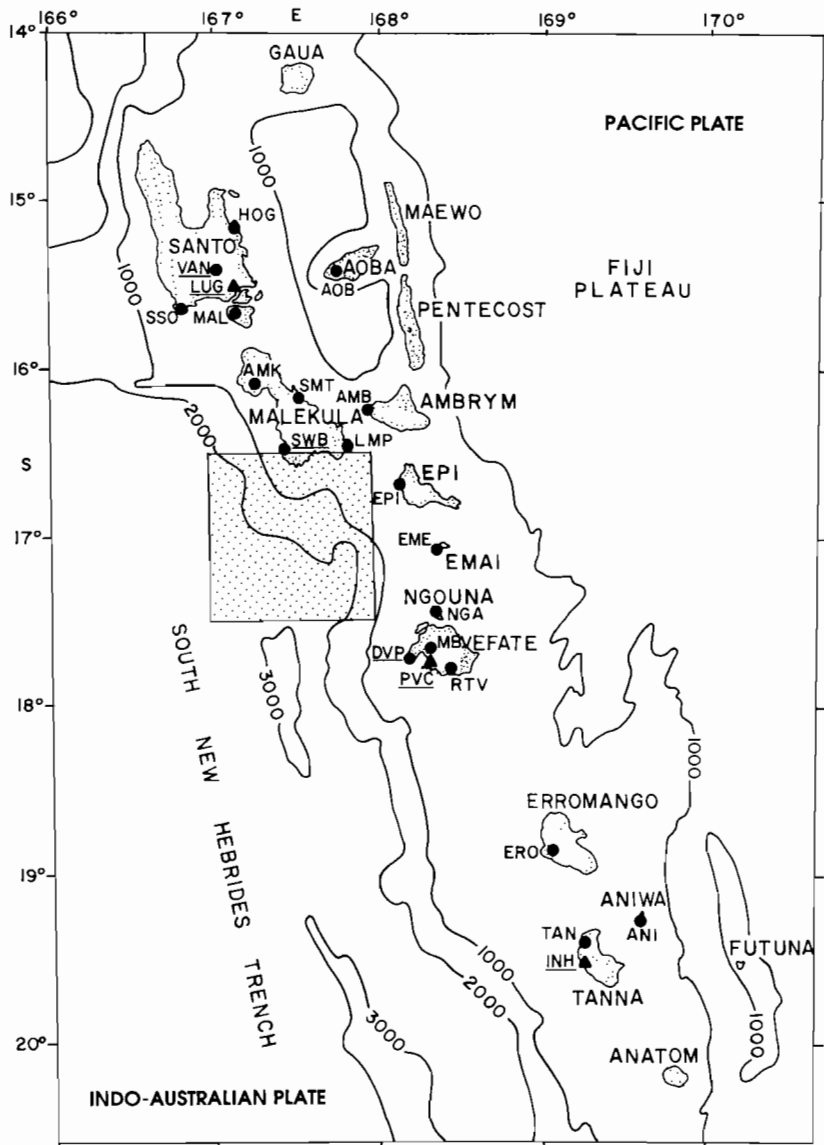


FIG. 1. Map of the central Hebrides island arc. The D'Entrecasteaux "fracture zone" is outlined by the westerly bend in the 2000 fathom contour. Stations of the ORSTOM/Cornell network are shown as solid circles. Underlined stations have a vertical and one horizontal component, while other stations have only a single vertical component. The region of anomalously located earthquakes is outlined in the shaded box between 16.5°S and 17.5°S.

The evolution of the structures in the central New Hebrides arc purportedly began with an episode of rifting in the late Miocene that resulted in the migration of Santo and Malekula to the west with the creation of the Aoba basin in the process (e.g., Karig and Mammereckx, 1972). This primary stage of extension was later replaced by one of compression, resulting in the uplift of the islands of Maewo and Pentecost along steep, reactivated normal faults that once bordered a graben (Mallick and Neef, 1974; Carney and Macfarlane, 1978; Isacks *et al.*, 1981). The emergence of the limestone reef caps on the islands of Efate, Erromango, and Aniwa to the south and on the Torres islands to the north may similarly be the result of

recent uplift (Mitchell and Warden, 1971; Bloom *et al.*, 1978; Bevis and Isacks, 1981). While feasible in many respects, however, this scenario is not unique and other mechanisms attributing most of the morphology strictly to interactions with the DFZ have been proposed (Chung and Kanamori, 1978a,b).

In contrast to the complicated structures and seismicity patterns that appear at the surface, the geometry of the deeper subduction zone is fairly regular. Cross-sections of teleseismically recorded earthquakes (Pascal *et al.*, 1978; Isacks and Barazangi, 1977) reveal a consistently simple pattern all along the arc, with the seismicity confined to a narrow, steeply dipping (70°) zone. Even so, a large aseismic region appears 70 km beneath the island of Efate that has been attributed to the subduction of the DFZ (Marthelot *et al.*, 1985).

As part of an investigation of the deep structure of the New Hebrides subduction zone (Roecker *et al.*; manuscript in preparation), we found that several locally recorded earthquakes were located beneath the trench at 60 to 90 km depth (Figure 2). Their epicenters are near the morphologically complex area where the DFZ interacts with Santo and Malekula. Because these locations are unusual and have important implications for our understanding of local tectonics and the rheology of the oceanic lithosphere, we investigated the accuracy of the reported locations in more detail.

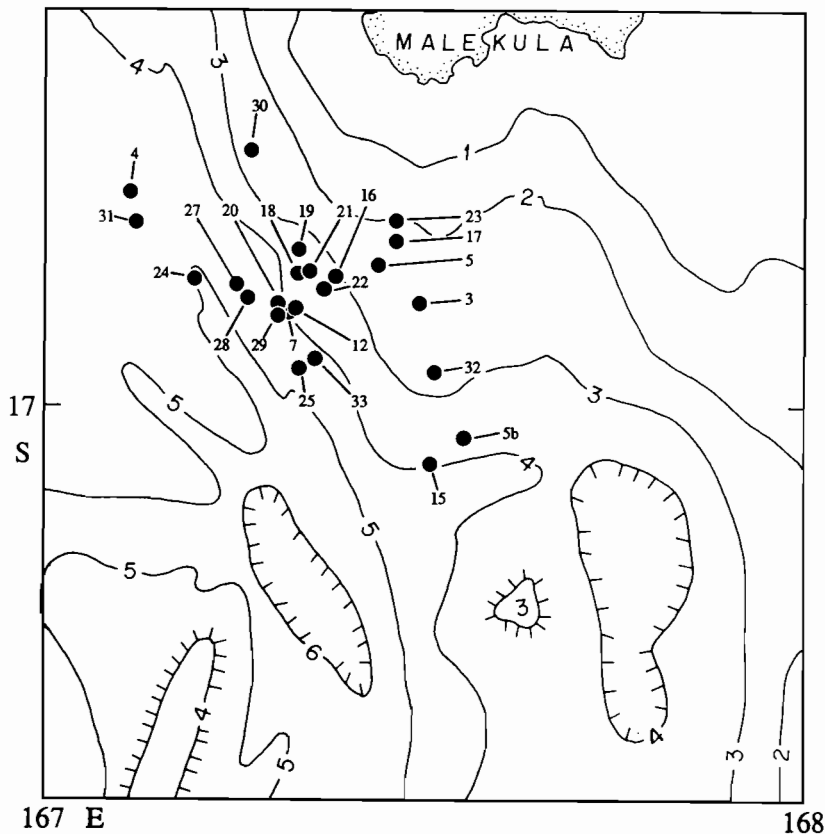


FIG. 2. Map of events located in the anomalous region by the ORSTOM/Cornell network. Bathymetric contours show depths in kilometers, adapted from Monzier *et al.*, 1984. Numbers identifying events correspond to those listed in Table 2.

DATA

The data used in this study are the arrival times of locally recorded *P* and *S* waves generated by earthquakes in the central New Hebrides subduction zone. Most of the arrivals were recorded by a network composed of 23 permanent land-based stations (Figure 1). Nineteen of these stations comprise a telemetered network installed and operated since 1978 by the Office de la Recherche Scientifique et Technique Outre-Mer (ORSTOM) and by Cornell University. The remaining four stations (Luganville (LUG), Port Villa (PVC), Noumea (NOU), and Koumac (KOU)) are drum recorders operated by ORSTOM. All of these stations are equipped with short period (1 Hz or 4.5 Hz) vertical seismometers, and several have one horizontal component as well.

All of the arrival times were originally read by ORSTOM technicians, and those recorded from the 22 anomalous earthquakes discussed in this paper, with the exception of those reported by station PVC, were reread by one of the authors (Roecker). In general, the *P* arrivals have an estimated precision of 0.05 sec, although some stations are generally less precise (e.g., PVC). The precision of *S* arrivals varies from station to station, depending on the existence of a horizontal component, among other factors. Impulsive *S* arrivals recorded on horizontal seismometers are estimated to have a precision of 0.05 sec. Less precise readings are also used in locating the events but are weighted accordingly.

Approximately 17,000 local earthquakes have been located using data from the New Hebrides network from 1978 to 1983. The 22 earthquakes discussed in this paper were taken from a dataset of 650 events that was culled from the initial set of 17,000 for the purpose of determining the elastic wave velocity structure of the subduction zone. Because location accuracy is crucial to the determination of velocity structure, the locations in the 650 event dataset had to satisfy a number of criteria in order to be selected. These criteria have some bearing on defining patterns in seismicity, and therefore we will briefly review the selection procedure.

As a first filter, we kept only those events that ostensibly were well recorded (more than eight total arrivals with a minimum of three *S* waves). These events were then relocated in two different one-dimensional structures and the subsequent locations were compared. Events were eliminated from further consideration if (1) the associated root mean square (RMS) residual was greater than 1 sec, (2) the condition number (the ratio of largest to smallest eigenvalue) of the matrix of location partial derivatives was greater than 80, or (3) the locations in the two different assumed structures differed by more than 10 km in any direction.

This selection procedure helps to ensure that only the better constrained earthquake locations are included, and, as our goal is to investigate the existence of earthquakes in the region of anomalous depths, we worked exclusively with this selected dataset. At the same time, a search through the entire location catalogue revealed that while roughly twice as many earthquakes occurred in the anomalous region than are discussed here, the exclusion of the less well constrained locations does not misrepresent the seismicity in this area.

ANALYSIS

The task of accurately locating an earthquake is not a trivial one, because a location depends in a complicated way upon the geometry of the recording stations, the phases reported, and the velocity structure assumed. Indeed, given an appropriately pathological velocity structure one can locate a given earthquake virtually

anywhere. Even in the realm of "reasonable" assumptions of velocity structure several pitfalls can occur. The purpose of this study is to determine if any of these pitfalls apply to the events located in the anomalous region below the trench.

As our data consist of arrival times of P and S phases, our primary criterion in judging the relative worth of a computed location will depend on the calculated fit to these times. If $\mathbf{t}_c = g(X, Y, Z, T)$ is the theoretical relationship between the arrival time and the hypocentral coordinates, then we define the vector of arrival time residuals as $\mathbf{R} = \mathbf{t}_0 - \mathbf{t}_c$, where \mathbf{t}_0 are the observed arrival times. The standard deviation of the residuals, σ_d , is defined by

$$\sigma_d = \left[\frac{\hat{\mathbf{R}}^T \mathbf{C}_{dd}^{-1} \hat{\mathbf{R}}}{n - 4} \right]^{1/2} \quad (1)$$

In this equation n is the number of observations, \mathbf{C}_{dd} is the data covariance matrix, and $\hat{\mathbf{R}}$ is the demeaned residual vector, defined by

$$\hat{\mathbf{R}} = \mathbf{R} - \frac{\sum_{i=1}^n w_i R_i}{\sum_{i=1}^n w_i} \quad (2)$$

where

$$w_i = \sum_{j=1}^n [\mathbf{C}_{dd}]_{ij}^{-1} = \frac{1}{\sigma_{ni}^2} \quad (3)$$

where σ_{ni}^2 is the variance of observation i , and the data errors are assumed to be uncorrelated.

To estimate the uncertainties in the locations, we use the nonlinear inverse theory of Tarantola and Valette (1982). Among other advantages, this theory does not require the assumption of linearity in error estimation, and prescribes a method for determining the effects of error in the theory on variable estimation. Tarantola and Valette (1982) showed that the *a posteriori* information density function (σ) for the hypocenter problem can be represented by

$$\sigma(X, Y, Z, T) = \rho(X, Y, Z, T) \exp \left[-\frac{1}{2} [\mathbf{t}_0 - g(X, Y, Z, T)]^T (\mathbf{C}_{dd} + \mathbf{C}_{mm})^{-1} [\mathbf{t}_0 - g(X, Y, Z, T)] \right] \quad (4)$$

where $\rho(X, Y, Z, T)$ is the *a priori* information density function and \mathbf{C}_{mm} is a covariance matrix that estimates the errors made by the theory. Equation (4) can be integrated analytically to obtain

$$\sigma(X, Y, Z) = K \rho(X, Y, Z) \exp \left[\frac{-\hat{\sigma}_d^2}{2} \right] \quad (5)$$

where

$$\hat{\sigma}_d^2 = \hat{\mathbf{R}}^T (\mathbf{C}_{dd} + \mathbf{C}_{mm})^{-1} \hat{\mathbf{R}} \quad (6)$$

The w in equation (2) is now

$$w_i = \sum_{j=1}^n [\mathbf{C}_{dd} + \mathbf{C}_{mm}]_{ij}^{-1} \quad (7)$$

and

$$K = \sum_{i=1}^n w_i \quad (8)$$

In the following we will assume no *a priori* information about the hypocenter other than requiring a positive depth, and therefore

$$\begin{aligned} \rho(X, Y, Z) &= 1 & Z \geq 0. \\ &= 0 & Z < 0. \end{aligned} \quad (9)$$

We will also assume that the variance of the error due to the theory is the same for all raypaths, and that there is no correlation of this error between raypaths. Therefore,

$$\mathbf{C}_{mm} = \sigma_m^2 \mathbf{I} \quad (10)$$

Marginal *a posteriori* density functions for depth and epicenter can be calculated by integrating $\sigma(X, Y, Z)$

$$\sigma(Z) = \int_{-\infty}^{\infty} dX \int_{-\infty}^{\infty} dY \sigma(X, Y, Z) \quad (11)$$

$$\sigma(X, Y) = \int_0^{\infty} dZ \sigma(X, Y, Z) \quad (12)$$

Note that statistical quantities such as expected values and covariances may be calculated from σ by integrating over weighted values. However, because there is more information in the density function itself, we will confine the discussion to the behavior of σ .

All of the locations and travel-time residuals were determined using an algorithm written by one of the authors (Roecker) that traces rays through a one-dimensional structure. We assumed two different one-dimensional velocity structures (Table 1) in testing the locations. The first model was a compilation of results of various investigators (Dubois, 1969; Kaila and Krishna, 1978; Ibrahim *et al.*, 1980) that was used by Coudert *et al.* (1981) to locate earthquakes in the New Hebrides. Information about S wave velocities (V_s) for this model is limited, although Coudert *et al.* (1981) determined an overall value of 1.75 for V_p/V_s . Recent plots of $\Delta S - S$ versus $\Delta P - P$ (Chatelain, 1978; Coudert *et al.*, 1981) using several tens of thousands of data points (Chatelain, personal communication) reveal V_p/V_s values ranging from 1.75 to 1.78, with the 1.78 value preferred by events located north of 17°S . We tried a variety of V_p/V_s ratios from 1.72 to 1.78 in conducting the tests using this model. For reasons explained below we will discuss in detail only the results of the tests using a V_p/V_s ratio of 1.78.

The second one-dimensional structure used (Table 1) is one determined by a least-squares fit of the arrival time residuals from the 650 earthquakes discussed above. The procedure used in determining this structure is discussed in detail by Roecker et al. (manuscript in preparation). Note that the V_p/V_s ratios change with depth in this structure, and feature a particularly high ratio (1.88) in the upper 12 km. This model also includes travel time corrections for each station (Table 2) to account for laterally varying structure (mostly near the receiver). These corrections are the average residuals at a station calculated from the set of 650 events located in the best fitting one-dimensional structure.

Because the 22 events discussed in this study are part of the dataset that was used to determine a three-dimensional velocity structure, they have been relocated in many more velocity models than those discussed here, including some that vary laterally. The relocations of these events were within about 10 km of their starting location of all of these models. We note therefore that it is not the case that the locations of these events are so imprecise that they may be equally well located

TABLE 1
ONE-DIMENSIONAL VELOCITY MODELS USED IN THE ANALYSIS
OF THE HYPOCENTERS IN THE ANOMALOUS ZONE

Coudert Model				Best Fit Model			
V_p (km/sec)	V_s (km/sec)	Depth (km)	V_p/V_s	V_p (km/sec)	V_s (km/ sec)	Depth (km)	V_p/V_s
5.20	2.92	0	1.78	5.49	2.92	0	1.88
7.20	4.04	12	1.78	6.81	3.89	12	1.75
8.06	4.53	30	1.78	7.62	4.28	30	1.78
8.13	4.57	100	1.78	7.97	4.58	45	1.74
8.17	4.59	200	1.78	8.22	4.61	60	1.78
8.20	4.61	240	1.78	7.37	4.31	75	1.71
				8.20	4.60	100	1.78
				8.39	4.55	150	1.84

TABLE 2
LOCATIONS OF STATIONS USUALLY USED IN CALCULATING THE
LOCATIONS OF EVENTS IN THE ANOMALOUS REGION, ALONG
WITH CORRECTIONS TO *P* AND *S* WAVE TRAVEL TIME USED IN
LOCATING EVENTS IN THE BEST FITTING ONE-DIMENSIONAL
MODEL

Station	Latitude (°S)	Longitude (°E)	Elevation (m)	P Corr. (s)	S Corr. (s)
LMP	16 28.32	167 49.18	138	-0.24	-0.20
SWB	16 30.52	167 25.22	305	-0.07	0.16
AMK	16 5.10	167 12.40	610	0.17	0.93
AMB	16 14.75	167 55.40	294	0.18	0.60
EME	17 5.45	168 21.07	527	0.03	0.16
EPI	16 41.70	168 6.97	188	0.12	0.38
NGA	17 27.12	168 20.42	593	-0.09	0.06
MBV	17 39.52	168 18.63	471	0.13	0.51
RTV	17 47.55	168 25.48	99	0.16	0.44
DVP	17 43.52	168 11.22	77	-0.09	0.12
PVC	17 44.40	168 18.72	77	-0.20	-0.10

anywhere between the surface and 90 km or deeper. However, there may exist other minima that the location procedure avoided because of the starting location (which is deep in this case) assumed. Therefore, the focus of this study is not on the absolute accuracy of the locations of the anomalous earthquakes, but rather on whether or not these earthquakes are deep (60 to 90 km) or shallow (<10 km).

In testing the hypocenters we first tried locating the events using a variety of starting depths from the surface to 110 km. In most cases the event was relocated at the same (deep) depth that was originally reported, but in several cases, usually when a shallow starting depth was assumed, the event moved upward and tried to locate above the surface. This behavior indicated that a possible alternate residual minimum existed at shallow depths.

To determine the characteristics of this alternate minimum, we next relocated the events with their depths fixed at various starting depths. (This was done by eliminating the depth term from the system of equations rather than by resetting the depth correction to zero. We found that a better fit to the data was often achieved by using the former method.) The results (Table 3, Figures 3 and 4) show that while some events (e.g., 4, 5, 31) have a single minimum, most of the events in the anomalous region have two. (Note that in most cases the shallow "minimum" is not really a minimum in the sense that the derivative of standard deviation with depth is zero, although the deviations for most events are the same to three digits for locations at 1 km depth and at the surface. For convenience we will refer to the decrease in standard deviation at shallow depths as a minimum. We also note that the ocean is 4 to 5 km deep in the anomalous region, and therefore very shallow depths are nonphysical.) Moreover, while some of the events with two minima are fit more or less equally well at either depth (e.g., events 7 and 24), most are better fit at the deeper depth.

There are two potential causes for the double minima: either the errors in the data are conspiring to produce a "false minimum" or the distribution of stations is such that the travel-time surface actually has two minima. The former is unlikely because of the similarity in the curves of standard deviation versus depth for several events. To demonstrate the latter possibility we generated hypothetical data for event 3, assuming first that it was at the surface and then at a depth of about 80 km (Figure 5). Both of these curves reveal double minima, which confirms our suspicion of a real double minima in the travel-time surface.

The reason for this double minima appears to be the absence of stations directly above and surrounding the hypocenter. A deep event will be recorded only in the upper focal sphere by a local network, which means that all of the partial derivatives of travel time with respect to depth are positive. Therefore, if the event is displaced toward the surface, the resulting negative residuals will push the event deeper. This effect becomes more pronounced at increasingly shallower depths, resulting in progressively worse fits to the data. However, as the event approaches the surface, it reaches a depth where all of the rays leave the bottom of the focal sphere, and the depth partial derivatives are now entirely negative. Now the early arrivals require a shallower depth to be fit and the standard deviation decreases with decreasing depth. We note that this effect could be alleviated if (1) there were a station directly above the hypocenter to ensure that at least one depth derivative remained positive and (2) there were stations surrounding the hypocenter to prevent the epicenter from migrating to a region where all of the rays are downgoing. Without data from stations in these strategic locations, some ambiguity will exist in any determination of hypocenter depth in this region west of the network.

TABLE 3
SUMMARY OF EVENT RELOCATIONS AT DIFFERENT DEPTHS

Event No.	Date	Time	Latitude (°S)	Longitude (°E)	Coudert Model					Best Fit Model					No. Phases		
					D1 (km)	STD1 (sec)	D2 (km)	STD2 (sec)	% IMP	D1 (km)	STD1 (sec)	D2 (km)	STD2 (sec)	% IMP	P	Tot.	
* 4	79/07/11	14:56	16.73	167.11	25.0	0.383					28.7	0.389				11	19
* 5	79/07/27	16:16	16.82	167.43	40.7	0.455					44.9	0.497				11	20
7	79/10/27	02:02	16.88	167.31	56.5	0.227	2.5	0.362	37	43.8	0.245	7.5	0.275	11		8	13
12	81/07/16	04:36	16.87	167.32	80.8	0.255	1.0	0.628	59	73.5	0.233	1.0	0.373	38		7	10
3	81/07/18	08:36	16.87	167.49	90.0	0.257	1.0	0.821	69	90.0	0.260	1.0	0.658	60		8	14
15	81/07/18	08:42	17.07	167.50	81.9	0.394	1.0	0.605	35	76.0	0.377	1.0	0.419	10		7	12
16	81/07/18	09:17	16.83	167.37	66.5	0.385	2.5	0.577	33	59.2	0.381	2.5	0.453	16		6	9
17	81/07/18	20:57	16.79	167.45	74.4	0.251	2.5	0.891	72	66.7	0.205	1.0	0.396	48		4	8
5b	81/07/18	22:54	17.04	167.55	80.0	0.201	1.0	0.414	51	80.0	0.135	1.0	0.291	54		7	14
18	81/07/20	11:27	16.83	167.33	67.2	0.270	2.5	0.729	63	60.7	0.252	1.0	0.391	35		5	10
19	81/07/20	16:43	16.80	167.33	71.3	0.566	2.5	0.845	33	62.9	0.461	1.0	0.536	14		7	12
20	81/07/21	23:55	16.87	167.30	70.7	0.485	1.0	0.623	22	66.5	0.408	5.0	0.556	27		7	12
21	81/07/22	10:26	16.82	167.34	68.6	0.369	0.0	0.880	58	61.4	0.467	1.0	0.520	10		5	7
22	81/07/22	21:19	16.85	167.36	69.5	0.322	2.5	0.619	48	63.1	0.286	5.0	0.518	45		6	11
23	81/07/25	06:07	16.76	167.45	72.2	0.245	1.0	0.536	54	68.5	0.260	1.0	0.404	36		7	13
24	81/07/25	19:50	16.83	167.19	61.4	0.221	1.0	0.224	1	57.1	0.197	1.0	0.252	22		5	8
25	81/07/25	21:09	16.95	167.33	72.9	0.309	1.0	0.444	30	66.8	0.340	2.5	0.413	18		7	10
27	81/08/01	02:19	16.84	167.25	58.7	0.386	2.5	0.479	19	50.4	0.340	7.5	0.404	16		8	13
28	81/08/01	06:07	16.86	167.26	55.7	0.298	5.0	0.416	28	43.7	0.238	7.5	0.287	17		7	13
29	81/08/02	01:11	16.88	167.30	70.9	0.213	2.5	0.435	51	64.1	0.176	5.0	0.360	51		8	16
30	81/08/05	10:43	16.67	167.26	66.8	0.345	5.0	0.780	56	61.6	0.231	5.0	0.563	59		8	13
* 31	81/08/08	20:56	16.76	167.11	27.4	0.369				30.4	0.518					10	15
* 32	81/07/19	00:55	16.96	167.51	1.0	0.714				5.0	0.537					5	9
* 33	81/07/27	06:06	16.94	167.36	1.0	0.387				7.5	0.292					5	9

Epicenters in columns 4 and 5 are for the deeper hypocenter. The depths and standard deviations for the deeper depths are given in columns labeled D1 and STD1, while those for shallower depths are in D2 and STD2. The last two columns give the number of P phases and the total number of phases reported, respectively. Events preceded by an asterick had only one depth minimum. Events 32 and 33 are shallow events included as a control.

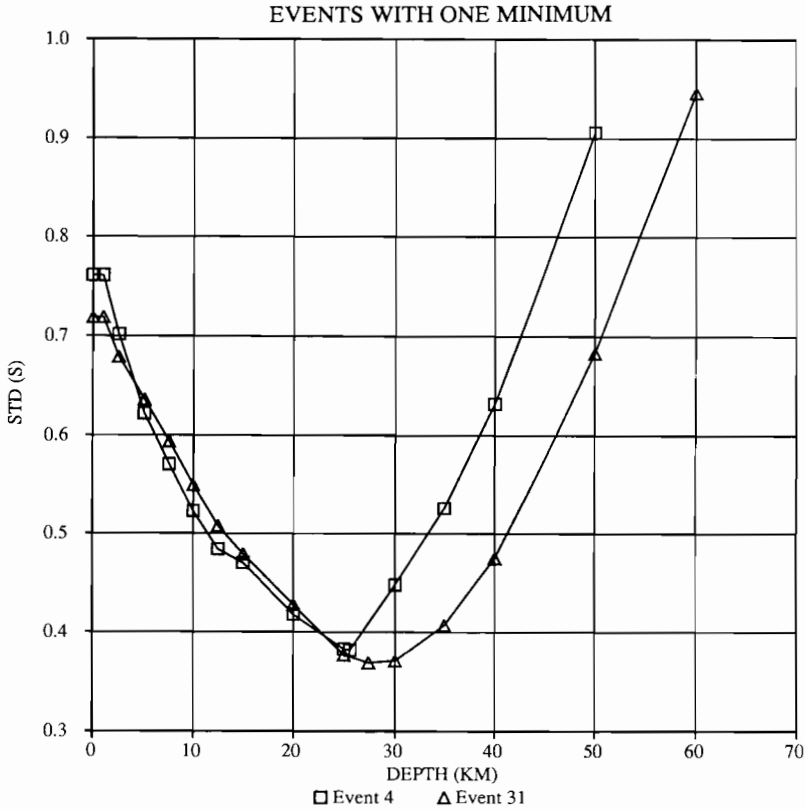


FIG. 3. Plot of standard deviation of residuals versus depth of event for two events whose data had only one minimum in the travel-time surface.

DISCUSSION

Despite the inherent ambiguity in the depth of these events, there are several observations that favor a deep depth for these events over a shallow one. In this section we review these observations.

Residual standard deviations. Plots of standard deviation versus depth for several events located in the Coudert model show a better fit at the deeper depths (Figure 4A, Table 3). Moreover, the discrepancy in fits increases with decreasing values of V_p/V_s . A comparison of the residuals produced by deep and shallow locations (Figure 6, Table 4) shows that while arrivals at distant stations are fit equally well at either depth, S waves at stations, SWB, LMP and DVP, the closest stations to the epicenter, are much better fit (0.1 sec versus 0.5 sec residuals) with the deeper hypocenter.

We observe that these large, consistently negative S residuals could be explained by a higher V_p/V_s ratio at shallow depths, and high ratios are predicted by the best fitting one-dimensional structure (Table 1). Relocations in this structure, with station corrections applied, usually reduced the standard deviation for both deep and shallow locations (Table 3, Figure 4b), but while the percent improvement in standard deviation at the deeper depth is less with this model, the deeper depths still provide a better fit. Moreover, for some events (20, 22, 29, and 30) the S residuals at SWB and LMP were still several tenths of a second at shallow depths.

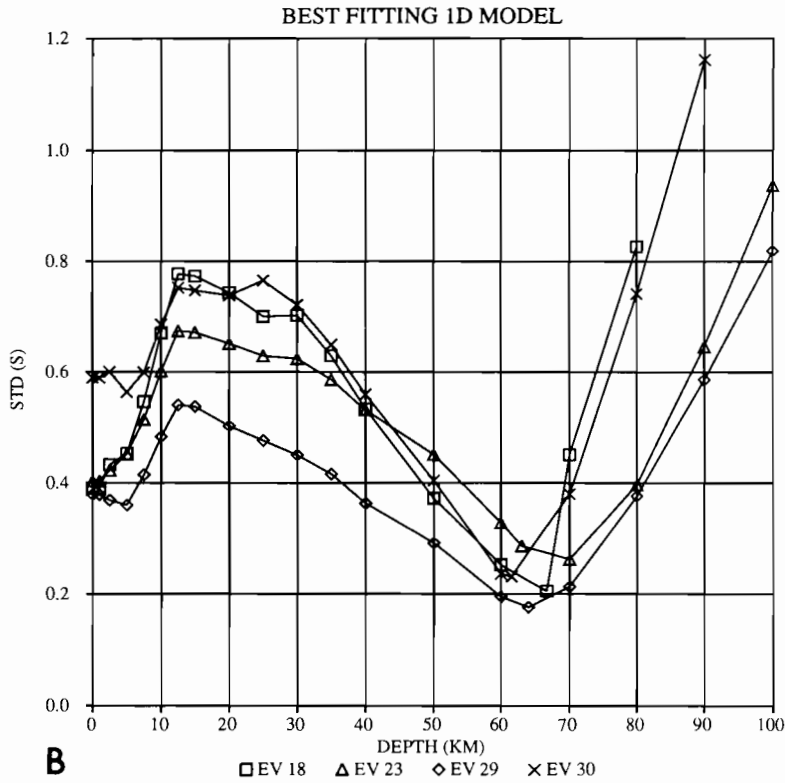
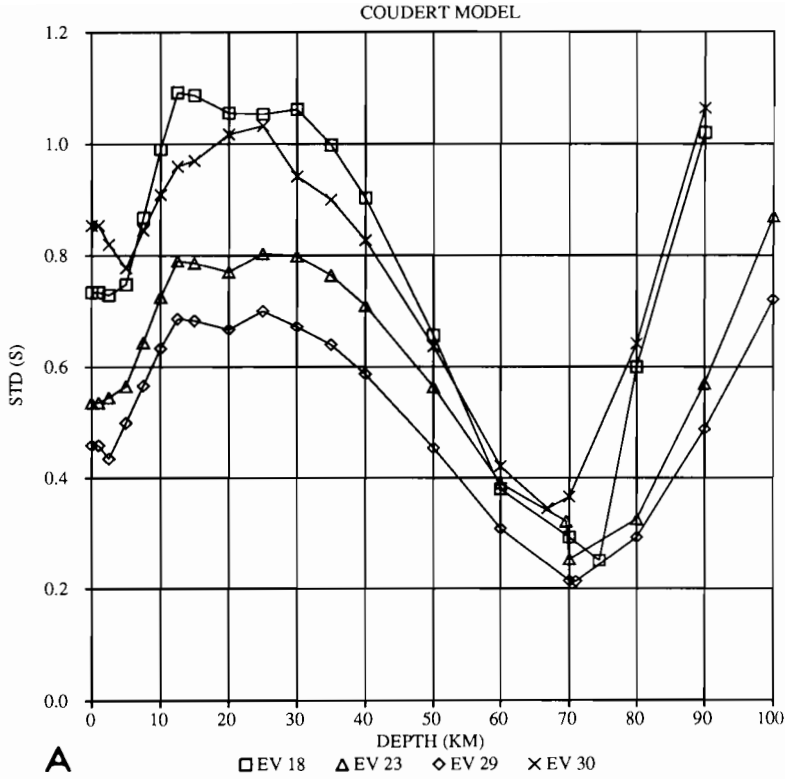


FIG. 4. Plots of standard deviation versus depth for four events whose data had two minima in the travel time surface. (a) Events located using the Coudert model. (b) Events located using the best fitting one-dimensional model with station corrections.

Note that not every event with a hypocenter in this region exhibits that same dual minima characteristic that the deep events are shown to exhibit. We have found some events (e.g., 32 and 33 in Table 3) whose *P* and *S* arrival times show increasingly worse fits with changes in depth in either velocity model (Figure 7),

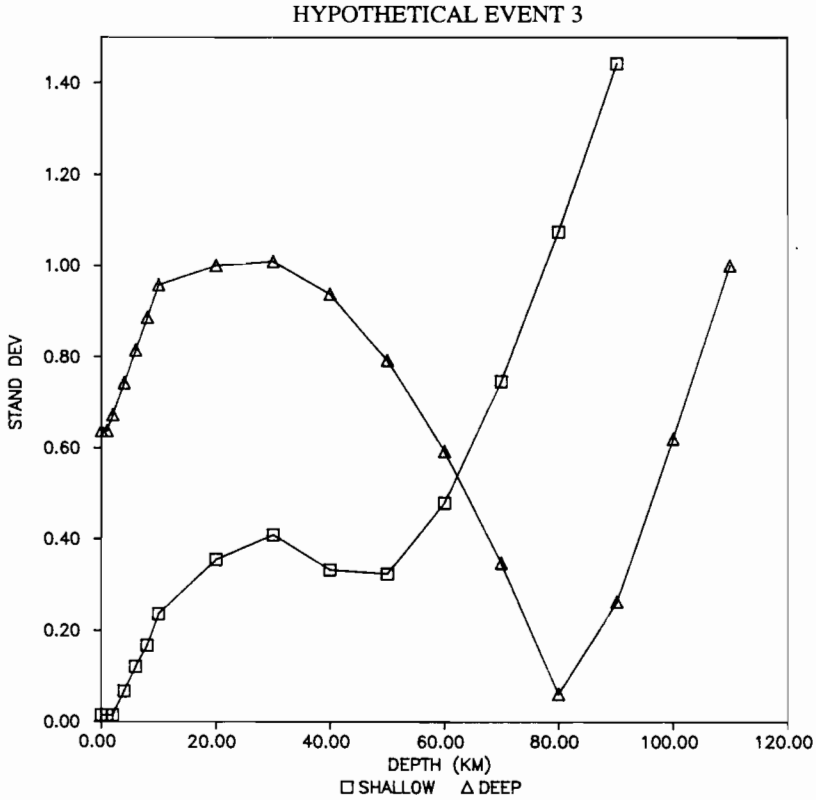


FIG. 5. Plots of standard deviation versus depth using hypothetical data from event 3 placed at 1 km depth (open squares) and 80 km depth (open triangles).

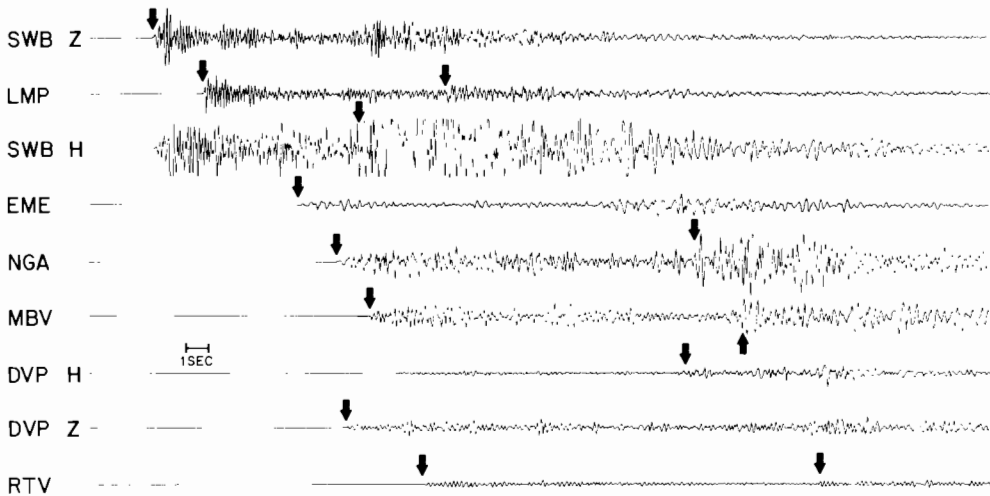


FIG. 6. Seismograms recording event 29. The picks used in the location of this event are indicated by the arrows.

TABLE 4
RESIDUALS AND RAY DIRECTIONS (U = UP; D = DOWN) OF *P*
AND *S* WAVES CALCULATED FOR EVENT 29

Station	Phase	Coudert Model				Best Fit Model			
		DEEP		SHALLOW		DEEP		SHALLOW	
		DIR	RES (S)	DIR	RES (S)	DIR	RES (S)	DIR	RES (S)
SWB	<i>P</i>	U	-0.01	D	0.18	U	-0.01	U	0.15
SWB	<i>S</i>	U	0.14	D	1.24	U	0.00	D	0.56
LMP	<i>P</i>	U	-0.01	D	-0.34	U	0.01	D	-0.21
LMP	<i>S</i>	U	-0.06	D	0.11	U	-0.08	D	-0.06
EME	<i>P</i>	U	-0.27	D	-0.29	U	-0.40	D	-0.24
EME	<i>S</i>	U	-0.50	D	0.23	U	-0.60	D	0.12
NGA	<i>P</i>	U	-0.15	D	-0.09	U	-0.08	D	0.11
NGA	<i>S</i>	U	0.47	D	1.33	U	0.64	D	1.42
MBV	<i>P</i>	U	0.20	D	0.15	U	0.07	D	0.09
MBV	<i>S</i>	U	0.32	D	0.98	U	0.10	D	0.60
DVP	<i>P</i>	U	-0.28	D	-0.16	U	-0.14	D	0.05
DVP	<i>S</i>	U	-0.87	D	0.10	U	-0.61	D	0.19
PVC	<i>P</i>	U	0.18	D	0.10	U	0.37	D	0.24
PVC	<i>S</i>	U	-0.48	D	0.01	U	-0.09	D	0.16
RTV	<i>P</i>	U	0.28	D	-0.19	U	0.05	D	-0.43
RTV	<i>S</i>	U	0.05	D	-0.04	U	-0.17	D	-0.51

Using the picks shown in Figure 9. Residuals are shown for the locations at the best fitting locations at deep and shallow depths as summarized in Table 3.

and therefore appear to have unambiguously shallow locations. Therefore, it is not the case that shallow events in this area will necessarily be better fit with a deeper hypocenter.

Marginal information density functions. The marginal *a posteriori* information density functions ($\sigma(Z)$ and $\sigma(X, Y)$) are related to the probability of a location being at a given point through the integration of the function in the vicinity of that point. For example, the probability *P* that the depth of an event is between *D* and *D* + δD is

$$P(D < Z < D + \delta D) = \int_D^{D+\delta D} \sigma(Z) dZ \quad (13)$$

Therefore, relative probabilities can be deduced by examining the areas under different parts of the σ curves. Examples of $\sigma(Z)$ and $\sigma(X, Y)$ are shown here for events 18 and 24 (Figures 8 and 9). Based on the analysis of residual standard deviations, event 18 is considered to be one of the better constrained locations, while event 24 is considered to be a poorly constrained location.

Note that in the absence of any error in the theory (Figure 8 and left side of Figure 9), the marginal information density functions reveal that the probability of the events being deep is significantly greater than it is for shallow depths, even for event 24. If we assume an error due to theory (σ_m) of 0.5 sec, which for these rays corresponds roughly to 5 per cent variations in the velocity structure (comparable to that determined by Roecker *et al.*, manuscript in preparation), the uncertainties are larger but the deeper depth still appears to be significantly more probable, especially for event 18 (Figure 8 and right side of Figure 9).

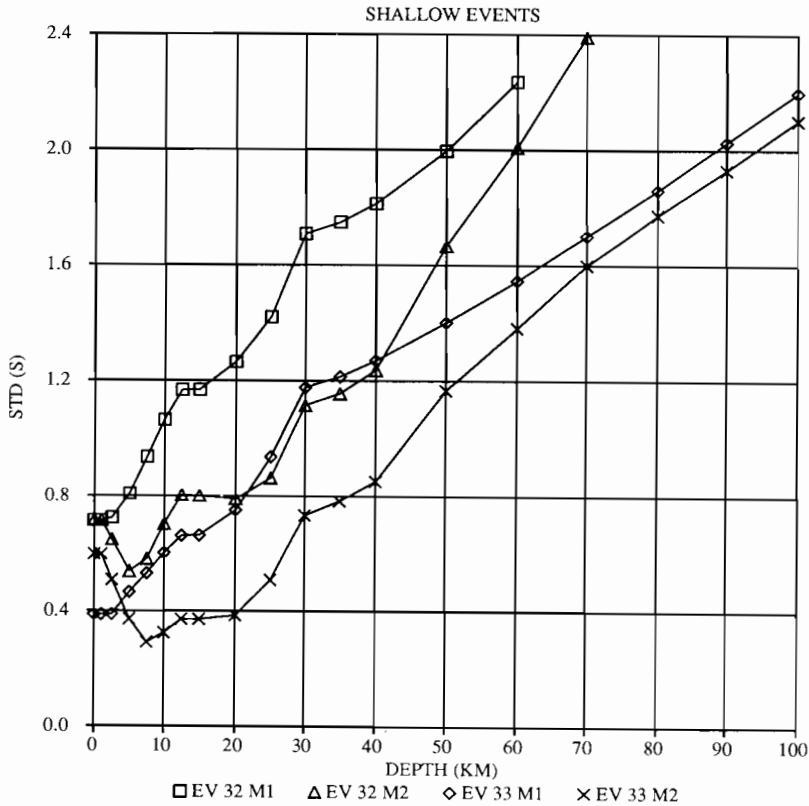


FIG. 7. Plot of standard deviation of residuals versus depth of event for events (32 and 33) that have a single minimum at shallow depth. M1 and M2 refer to locations in the Coudert and Best Fit models, respectively.

The reason why $\sigma(Z)$ appears to tell a more conclusive story than the standard deviations is that when comparing standard deviations we are comparing two values of $\sigma(X, Y, Z)$. However, equations (11) and (12) tell us that the likelihood of a given parameter is determined by an integration of σ over all other variables, and equation (13) shows that the actual probability is an integration of the marginal density function over a given range. Therefore, if the residual variance is small over a wide range of epicenters at one depth but over a narrow range of epicenters at a different depth, the former depth will be more probable. This is what appears to be happening to the residuals in the present case.

Coda excitation. An observation unrelated to travel times that supports deep locations is an apparent difference between shallow and deep events in the excitation of *S* coda at the station closest to the epicenters (SWB). All of the events with reported deep locations show a strong coda following the *S* wave recorded at SWB, especially on the horizontal component, while the coda from a shallow event appears to decay relatively rapidly (Figure 10). This difference in coda decay probably reflects a difference in attenuation environment, perhaps in the form of greater intrinsic attenuation (i.e., conversion to heat rather than scattering) at shallower depths. A noticeable difference in attenuation environment implies a significant difference in location for these events.

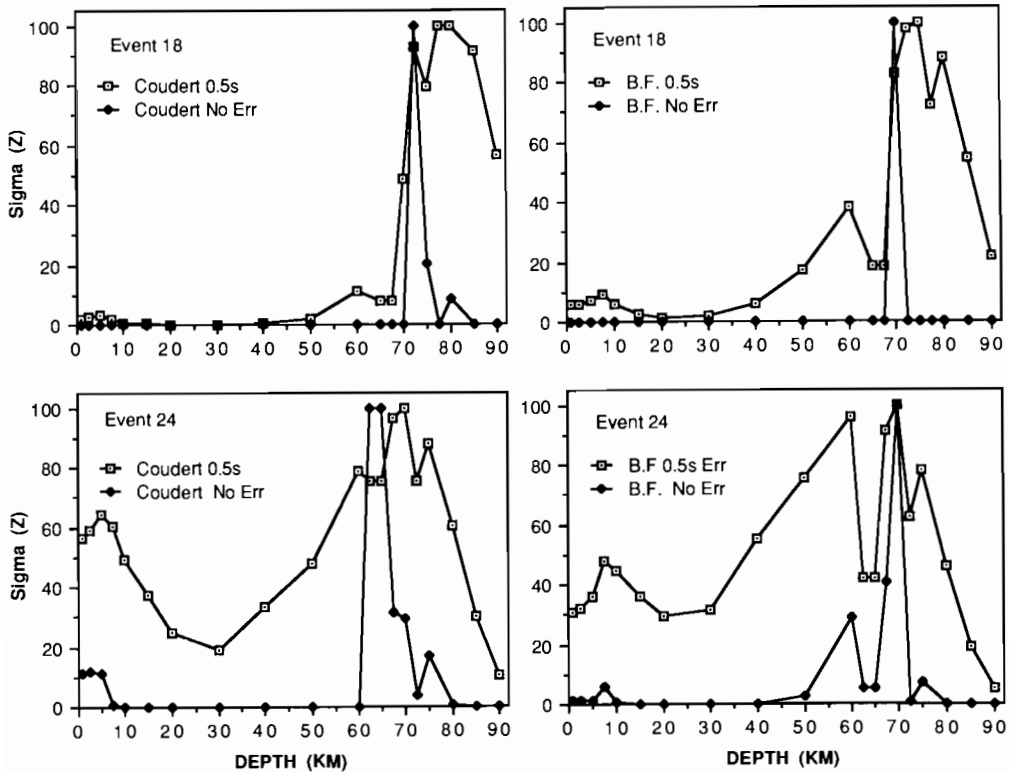


FIG. 8. Plots of $\sigma(Z)$ versus depth for events 18 (top) and 24 (bottom). Values of $\sigma(Z)$ have been normalized to 100. Values are shown for the Coudert (left) and Best Fit (right) models with no error in theory (closed diamonds), and with 0.5 sec. error in theory (open squares).

Teleseismic recordings. A final piece of evidence in favor of deep locations is that the Bulletin of the International Seismological Centre (ISC) lists 14 moderate sized ($M_b > 5.0$) earthquakes occurring in the anomalous area within one month of the main shock of July 15, 1981. The main shock was an interplate, thrust event located about 40 km to the southeast of the anomalous area at 17.26°S , 167.60°E with a strike of 349° , a dip of 11° and a slip of 90° (PDE bulletin, 1981). Ten of these aftershocks have depths greater than 25 km and five have depths in excess of 40 km (Table 5, figure 11). These earthquakes are significant for several reasons: (1) they provide an independent determination of deep earthquake locations in this region; (2) they show that large as well as small earthquakes occur in this region; and (3) they are located in a different velocity structure (with downgoing rays) than that assumed for the locally recorded events. These earthquakes thus provide some corroboration for our inference of deep earthquakes in this area.

Unfortunately, none of these events were well located with data from the local network (S waves are saturated at near stations). Also, because ISC depths are notoriously ill-constrained, especially for earthquakes with depths less than 75 km, these reports may be unreliable. We attempted to relocate several of the events using combined local and teleseismic P arrival times but found that, while the local P waves fit the teleseismic hypocenters reasonably well and produced only one minimum near the ISC reported depth, the improvements in depth constraints were

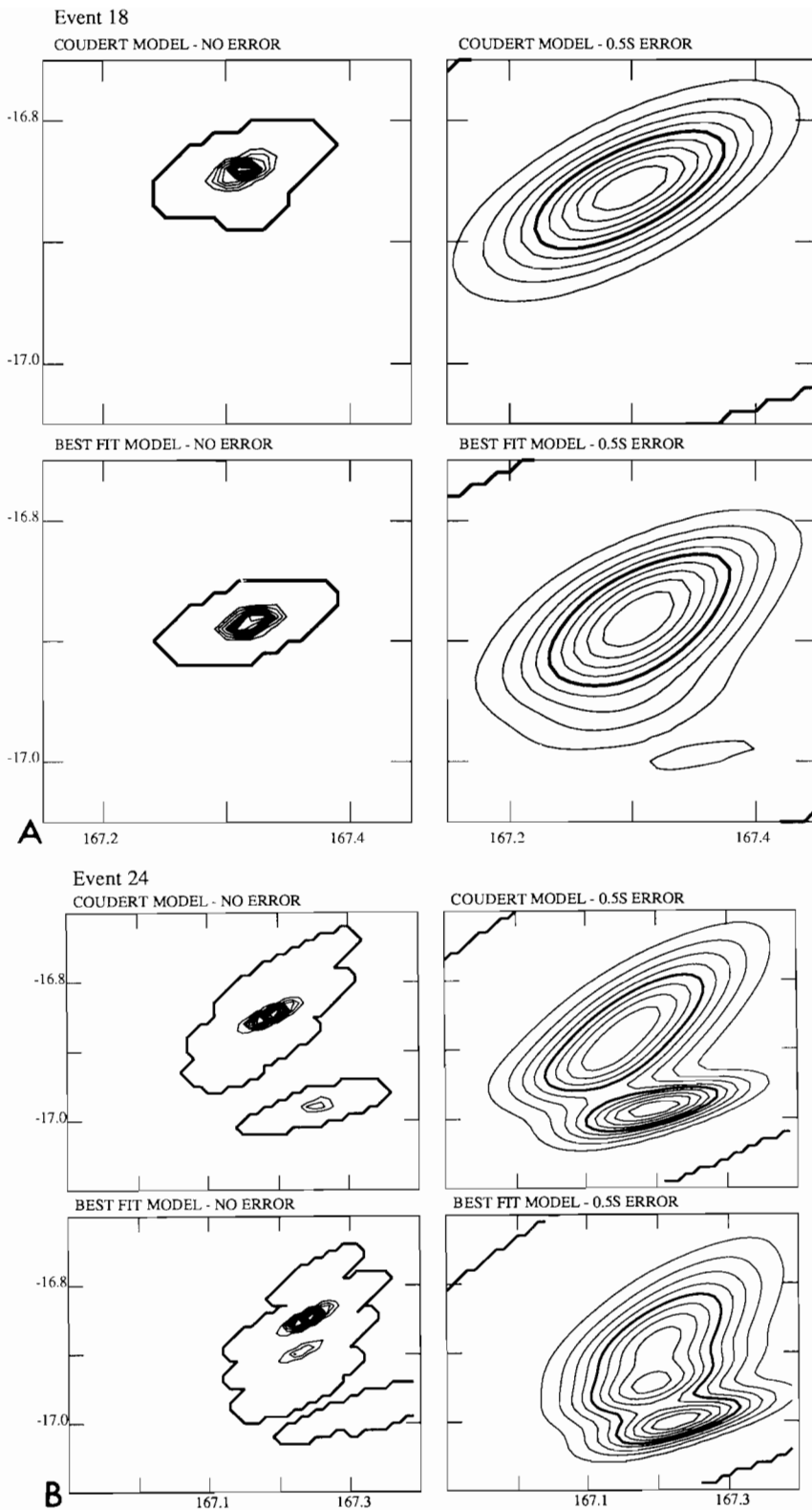


FIG. 9. Contours of $\sigma(X, Y)$ for the Coudert (upper) and Best Fit (lower) models with no error (left) and 0.5 sec. error (right) in the theory. The contour interval is 10 per cent. The heavy line on the outside of the contours is the computational zero, while the heavy line in the interior denotes the 50 per cent level. (a) Contours for event 18. The 10 per cent contour centered at -17.0° in the lower right plot is due to a decrease in variance at the shallow depth. (b) Contours for event 24. The northern maximum corresponds to the deep location and the southern maximum to the shallow location.

marginal (typically ± 15 km). We also attempted to determine the depths for some of these events using waveform modeling techniques but found that the waveforms were too complicated to be explained by a simple source in a one-dimensional structure. At the same time, we note that several of these events had *pP* times reported. We examined the records for the deepest of these events (event 12 of Table 5) and found that there was a distinct arrival close to the predicted *pP* arrival time (Figure 12 and Table 6). This observation strengthens our belief that these events are anomalously deep.

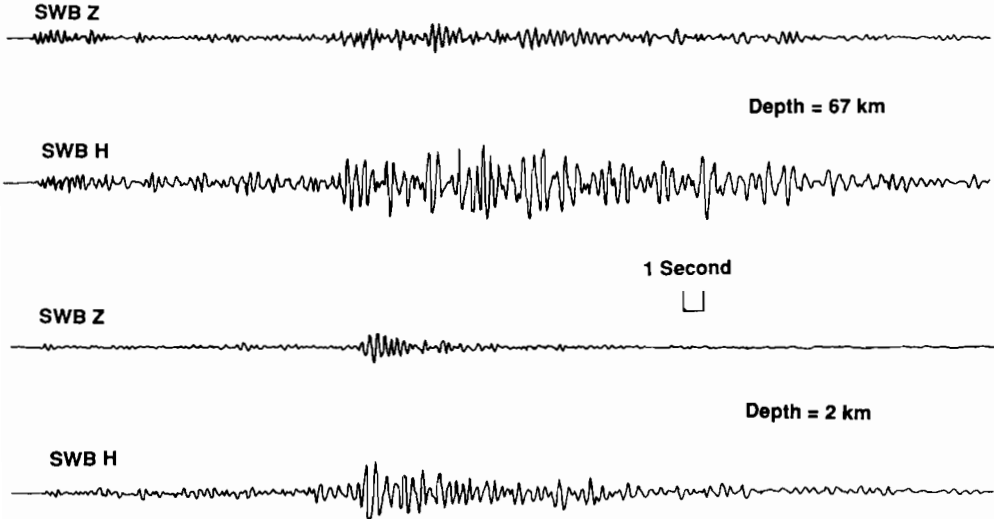


FIG. 10. Comparison of *S* coda recorded at vertical and horizontal seismometers at SWB from (a) a deep event (18) and (b) a shallow event (32).

TABLE 5
LOCATIONS OF LARGE EVENTS LOCATED IN THE ANOMALOUS REGION BY THE ISC

	Date	Time	Latitude (°S)	Longitude (°N)	Depth (km)	Mag (M_b)	NS
1	81/7/15	7:59: 9.7	17.29	167.59	28 \pm 2*	5.6	228
2	81/7/15	8: 8:46.8	17.13	167.32	92 \pm 15	5.0	21
3	81/7/15	8:15:51.1	17.34	167.71	44 \pm 8	5.4	91
4	81/7/15	8:28:17.9	17.28	167.63	54 \pm 11	5.3	69
5	81/7/15	8:39:35.9	17.39	167.69	47 \pm 18	5.0	68
6	81/7/15	9: 0:43.0	17.08	167.49	28 \pm 10	5.2	102
7	81/7/15	10: 1:19.5	16.96	167.42	29 \pm 5*	5.0	59
8	81/7/15	11: 5:32.6	17.39	167.66	15 \pm 14	5.2	140
9	81/7/15	15:21:55.0	17.05	167.26	33 \pm 1*	5.1	101
10	81/7/17	0:57:33.0	17.21	167.58	31 \pm 4*	5.0	112
11	81/7/18	0:26: 8.4	17.17	167.25	34 \pm 1*	5.1	66
12	81/7/19	4:42:59.0	17.16	167.58	45 \pm 1*	5.5	171
13	81/7/29	5: 9:12.6	16.79	167.19	28 \pm 15	5.0	72
14	81/7/31	0: 1: 1.4	16.75	167.44	21 \pm 12	5.2	46

Depths followed by an asterisk are those determined using *pP-P* picks. NS is the number of stations reporting the arrival.

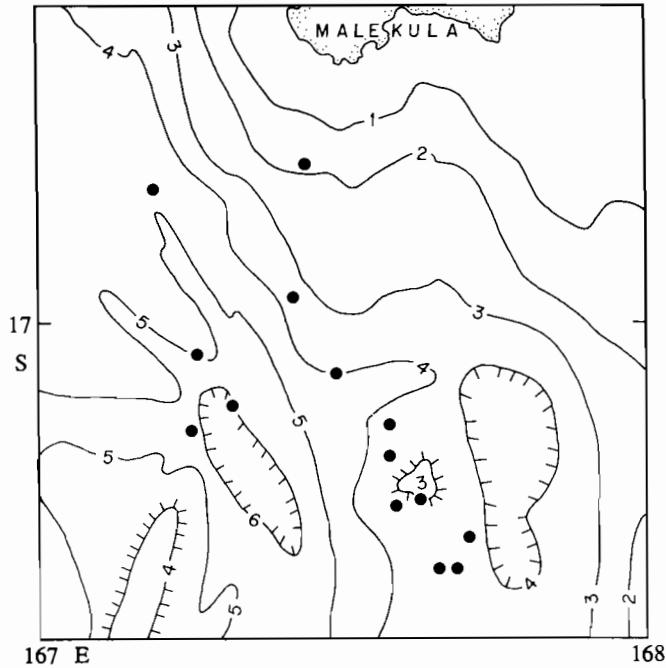


FIG. 11. Locations of aftershocks of the July 15, 1981 earthquake reported by the ISC Bulletin to have occurred in the anomalous zone.

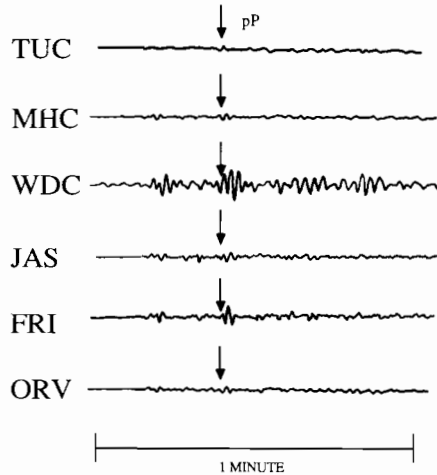


FIG. 12. Examples of seismograms from aftershock event 12 that reported pP times. Arrows denote the predicted arrival times of pP at these stations.

TECTONIC IMPLICATIONS

The oceanic lithosphere subducting beneath the New Hebrides is about 50 m.y. old (Weissel et al., 1981). If we assume that all subduction related seismicity in the central New Hebrides is occurring within the same piece of lithosphere, then a limiting temperature of 600° to 800°C for earthquakes to occur in the oceanic mantle (e.g., Bergman and Solomon, 1984; Weins and Stein, 1983, 1983) along with a normal geotherm for oceanic lithosphere (Parsons and Sclater, 1977) would imply that there should be no earthquakes beneath about 40 km depth in this area.

TABLE 6
STATIONS REPORTING PP TIMES FOR TELESEISMIC EVENT 12

Sta	Delta (°)	Azimuth (°)	pP Time	Residual (s)
KUR	64.63	345	4:53:46.00	-1.1
MHC	85.77	49	4:55:49.00	0.8
WDC	86.53	46	4:55:53.00	1.1
ORV	86.81	47	4:55:54.00	0.7
JAS	86.89	49	4:55:54.00	0.3
FRI	87.03	50	4:55:55.00	0.6
IRK	88.12	327	4:55:55.00	-4.3
MNV	88.73	49	4:56:03.00	0.4
SHW	89.19	41	4:56:05.40	0.8
GLA	89.24	55	4:56:05.60	0.5
BMN	90.17	48	4:56:10.00	0.6
TUC	92.19	57	4:56:19.70	0.8

Therefore, the existence of earthquakes at depths of 60–90 km (approximately the bottom of seismic lithosphere for 50 m.y.-old oceanic lithosphere) would suggest either that the temperature gradient is exceptionally lower than normal in this area, or that any of several parameters that could affect the rheology of the mantle, such as confining pressure, anomalous mineralogy, or the presence of fluids, is acting to depress the depth of the brittle-ductile transition. Given the uncertainties in our understanding of both the environment in which these earthquakes occur and the effects of various factors on the brittle-ductile transition (e.g., Paterson, 1987), we will not speculate on this class of causes for these deep events in any detail. At the same time, there are some simple observations that may have some bearing on the existence of these earthquakes.

First, the deep earthquakes beneath the trench are recorded only at a particular place along the entire arc, and then only infrequently as clusters of activity. Nineteen of the earthquakes investigated in this study are aftershocks of a large ($M_w = 7.1$) earthquake that occurred July 15, 1981, while three of them (4, 5, and 7) occurred within 3 months of each other in 1979. Such a localization of activity makes it doubtful that their existence reflects a depressed geotherm.

Another cluster of activity was reported to have occurred during March and April of 1986 in the same area as the events investigated in this study (Figure 13, Table 7). We attempted to perform the same analysis on the reported times of these events as was done on the earlier set, with the exception of not rereading the records, but found that the standard deviations in the travel times were either large at any depth (greater than 0.7 sec) or were virtually the same at deep and shallow depths. Unlike the 1981 events, the 1986 events were not associated with a mainshock. Therefore, while these events may not occur exclusively as aftershocks, they do occur infrequently and in clusters. The infrequent occurrence of events of this type would necessitate long-term monitoring to unambiguously define their existence. This may be why similar earthquakes have not been reported in other subduction environments.

As noted above, the epicenters of these events are in a structurally complicated part of the island arc. Bathymetric data (Monzier et al., 1986) show that the trench bends abruptly westward by 20° to 30° before it encounters the island of Malekula (Figure 14). Most of the earthquakes occur just to the north of this bend. These events also occur near an identified seismic discontinuity (boundary 2 of Chatelain

et al., 1986), and the epicenters of several events of the 1981 cluster, as well as most of those of the cluster in 1986, follow the trend of this boundary (Figures 13 and 14). Finally, while earthquakes with depths greater than 100 km tend to align along a N20°W azimuth, there is an offset in their locations north and south of the anomalous area (Figure 15c). Together, these observations imply an abrupt change

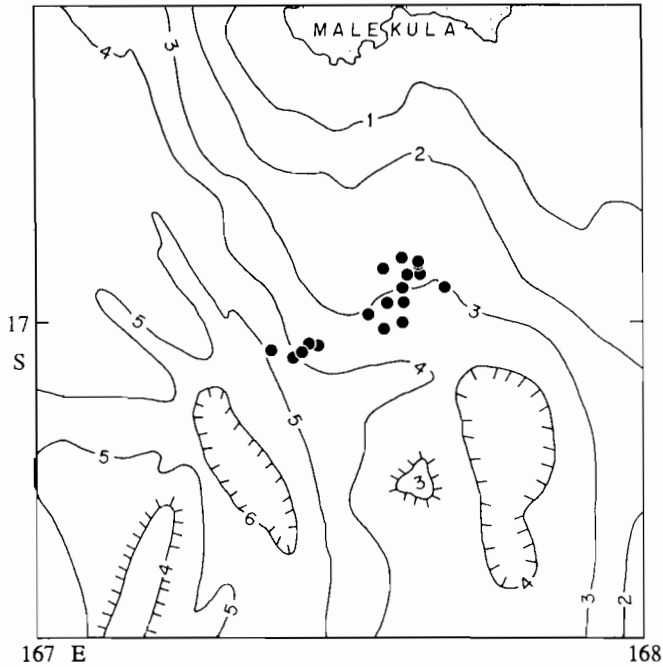


FIG. 13. Locations of events that occurred in March and April of 1986 in the same region as the 1981 aftershocks.

TABLE 7
LOCATIONS OF EVENTS IN 1986 THAT WERE REPORTED IN THE
SAME AREA AS THOSE IN 1981

Date	Time	Lat. (°S)	Long. (°E)	Depth (km)	No. Phases	
					P	Tot.
86/03/31	7:45	16.98	167.54	53.9	5	10
86/03/31	10:02	16.92	167.63	49.0	6	12
86/03/31	10:21	16.94	167.67	39.4	5	9
86/04/15	10:44	16.89	167.60	65.6	9	16
86/04/15	10:52	17.01	167.57	67.0	12	20
86/04/15	10:54	16.94	167.60	56.5	7	10
86/04/15	10:55	16.90	167.63	60.3	4	7
86/04/15	11:05	17.03	167.46	45.1	8	15
86/04/15	11:21	17.03	167.45	50.7	9	15
86/04/15	12:54	17.00	167.60	85.1	9	15
86/04/15	15:01	16.96	167.60	47.8	11	19
86/04/15	15:28	16.92	167.61	58.7	10	18
86/04/15	19:59	17.05	167.42	50.7	6	12
86/04/16	1:48	17.04	167.43	52.5	7	13
86/04/16	2:40	17.04	167.38	60.1	6	11
86/04/17	11:23	16.97	167.57	40.9	10	19
86/04/17	11:28	16.90	167.63	60.6	7	14
86/04/17	12:33	16.91	167.57	70.7	9	17

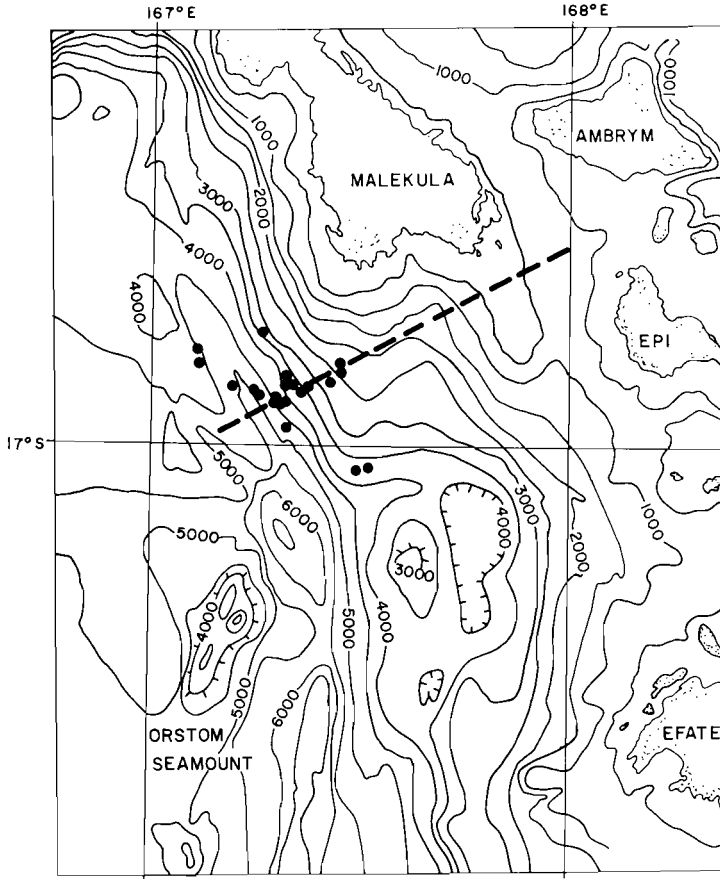


FIG. 14. Local bathymetry above the region of anomalous earthquakes, adapted from Monzier et al., 1984. Depths are contoured at 500 m intervals. Solid circles give the locations of the anomalous events. The thick dashed line marks the seismic boundary "2" of Chatelain et al. (1986).

in the environment of the subducted plate in this area, perhaps in the form of a tear in the downgoing plate.

The shallow seismicity in the central part of the arc is separated into two bands: one with a $N20^{\circ}W$ strike that parallels the island arc and one with a $N30^{\circ}W$ strike that parallels the western coasts of Santo and Malekula from the DFZ to the island of Efate (Figures 15a and 15b). The 30° trend extends from the surface down to the depths of the anomalous zone discussed here (60–90 km). Below this depth the seismicity follows the 20° trend exclusively. We also note that the anomalous zone is situated directly above a large seismic gap in the Wadati-Benioff zone that has been interpreted as a manifestation of the subducted DFZ (Marthelot et al., 1985). The existence of earthquakes at depths of 60–90 km therefore may be related to the interaction of the DFZ with the trench, and/or to the rifting episode that caused Santo and Malekula to drift towards the trench. For example, it could be that Santo and Malekula are causing the trench to "step back" to the west, so that the 30° trend is actually a manifestation of recent, en-echelon subduction. If this were the case then these events could be occurring at the top of the new slab, and their depths would not be anomalous. A cross-section of locations in the anomalous region (Figure 16) can be interpreted as conforming to this type of scenario.

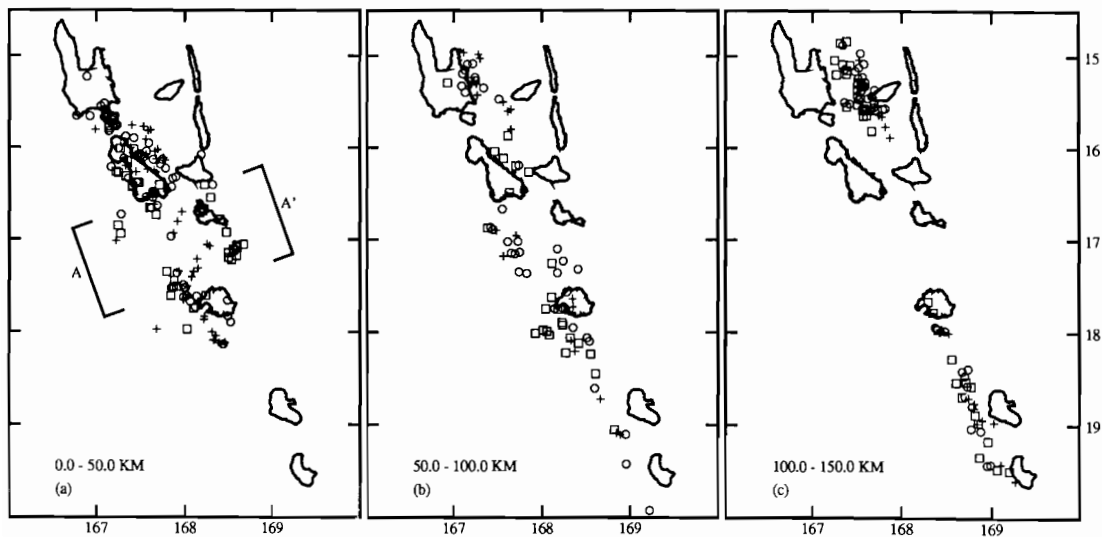


FIG. 15. Ambient seismicity of the New Hebrides, as determined by the 650 events in the selected dataset. In each map, the boxes, circles, and crosses refer to events in the upper, middle, and lower third, respectively, of the depth range shown in each figure. The anomalous events are located directly south of Malekula in Figure 15b. The brackets in 15a show the location of the cross-section in Figure 16.

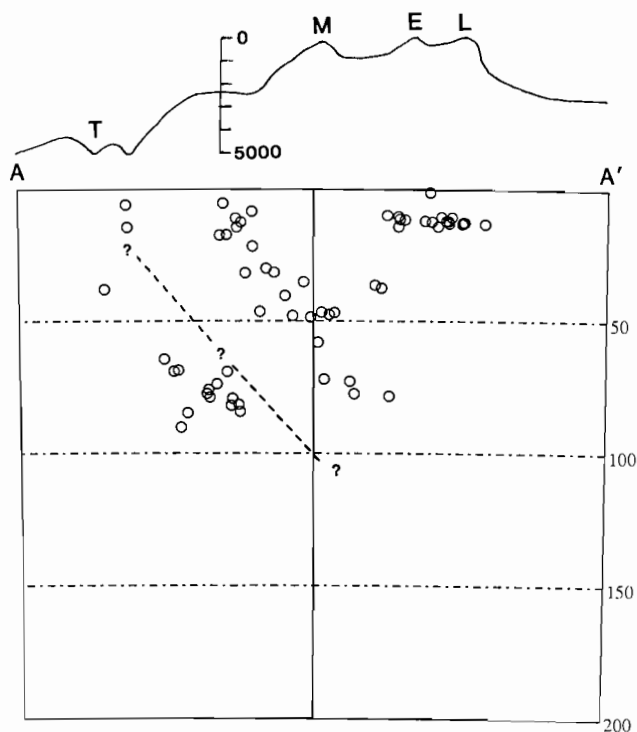


FIG. 16. Cross-section of seismicity in the region of anomalous depth earthquakes. The location of the section is shown in Figure 15a. Depths are in kilometers, and there is no vertical exaggeration. The vertical line locates the center of the section at 17°S , 168°E . A cross-section of local bathymetry is plotted at the top of the section. The anomalous earthquakes are located at the lower left, and the dashed line denotes an hypothesized en-echelon plate boundary.

While inviting in its simplicity, the above scenario belies the complexity of the tectonics of the region. The roles of features such as the seismic discontinuities mentioned above and a fault that runs through the Orstom seamount and intersects the trench near the location of the anomalous events (Daniel et al., 1986) presently are difficult to explain in other than an *ad hoc* fashion. The sporadic nature of the seismicity in this area is also unexplained. On the other hand, if this seismicity is not related to a new subduction boundary, then our understanding of the mechanics of the oceanic lithosphere is brought into question.

Therefore, while we do not fully understand the cause of these earthquakes at present, we feel that the unusual tectonics in this region is most likely a key factor. If nothing else, the probable existence of these earthquakes underscores the need for a sustained investigation employing OBS sensors to verify their locations.

ACKNOWLEDGMENTS

The local data used in this study were collected by ORSTOM members F. Bondoux, B. Campillo, C. Douglas, R. Foy, L. Mollard, D. Nakedau, and J. C. Willy. We thank them for their efforts. We also thank Geoff Abers, Kaye Shedlock, James Taggart, and Robert Uhrhammer for providing the teleseismic data. Discussions with and a review from W. Spence, along with comments from Charles Langston, were very helpful. This work was supported by National Science Foundation grant EAR-8407280, and by the Institut Francais de Recherche Scientifique pour le Developpement en Cooperation (ORSTOM).

REFERENCES

- Bergman, E. A., and S. C. Solomon (1984). Source mechanisms of earthquakes near mid-ocean ridges from body waveform inversion: implications for the early evolution of oceanic lithosphere, *J. Geophys. Res.*, **89**, 11415–11441.
- Bevis, M., and B. Isacks (1981). Leveling arrays as multicomponent tiltmeters: Slow deformation in the New Hebrides island arc, *J. Geophys. Res.*, **86**, 7808–7824.
- Bloom, A. L., C. Jouannic, and F. W. Taylor (1978). Preliminary radiometric ages from the uplifted Quaternary coral reefs in Efate, in *Geology of Efate and Offshore Islands*, R. P. Ash, J. N. Carney, and A. Macfarlane, Editors, Geological Survey, New Hebrides, 47–49.
- Carney, J. N. and A. Macfarlane (1978). Lower to middle Miocene sediments on Maewo, New Hebrides, and their relevance to the development of the outer Melanesian arc system, *Bull. Aust. Explor. Geophys.*, **9**, 123–130.
- Chatelain, J. L. (1978). *Etude fine de la sismicite en zone de collision continentale au moyen d'un reseau de stations portables: la region Hindu-Kush Pamir*, These docteur de 3e cycle, L'Universite scientifique et medicale de Grenoble, 219 pp.
- Chatelain, J. L., B. L. Isacks, R. K. Cardwell, R. Prevot, and M. Bevis (1986). Patterns of seismicity associated with asperities in the central New Hebrides island arc, *J. Geophys. Res.*, **91**, 12497–12519.
- Chung, W. Y. and H. Kanamori (1978a). A mechanical model for plate deformation associated with aseismic ridge subduction of the New Hebrides arc, *Tectonophysics*, **50**, 29–40.
- Chung, W. Y. and H. Kanamori (1978b). Subduction process of a fracture zone and aseismic ridges—the focal mechanism and source characteristics of the New Hebrides earthquake of January 19, 1969 and some related events, *Geophys. J.R. Astron. Soc.*, **54**, 221–240.
- Coudert, E., B. L. Isacks, M., Barazangi, R. Louat, R. Cardwell, A. Chen, J. Dubois, G. Latham, and B. Pontoise (1981). Spatial distribution and mechanisms of earthquakes in the southern New Hebrides arc from a temporary land and ocean bottom seismic network and from worldwide observations, *J. Geophys. Res.*, **86**, 5905–5925.
- Coudert, E., R. K. Cardwell, Bryan L. Isacks, and J. L. Chatelain (1984). P-wave velocity of the uppermost mantle and crustal thickness in the central Vanuatu islands (New Hebrides island arc), *Bull. Amer. Seism. Soc.*, **74**, 913–924.
- Daniel, J., C. Jouannic, B. Larue, and J. Recy, 1977. Interpretation of the D'entrecasteaux zone (north of New Caledonia), in *International Symposium on Geodynamics in South-West Pacific*, Noumea, New Caledonia, Editions Technip, Paris, 117–124.
- Daniel, J., J.-Y. Collot, M. Monzier, B. Pelletier, J. Butscher, C. Deplus, J. Dubois, M. Gerard, P. Maillet, M.-C. Monjaret, J. Recy, V. Renard, P. Rigolot, and S. J. Temakon (1986). Subduction et collisions le long de l'arc des Nouvelles-Hebrides (Vanuatu): resultats preliminaires de la campagne SEAPSO (Leg I), *C. R. Acad. Sci Paris*, **303**, 805–810.
- Dubois, J. (1969). *Contribution a l'etude structurale du Sud-Ouest Pacifique d'apres les ondes sismiques*

- observees en Nouvelle Calédonie et aux Nouvelles Hébrides*, these de doctorat es Sciences Physiques, Univ. de Paris, Paris, 160 pp.
- Dubois, J., J. Launay, J. Recy, and J. Marshall (1977). New Hebrides trench: Subduction rate from associated lithospheric bulge, *Can. J. Earth Sci.*, **14**, 250-255.
- Ibrahim, A., B. Pontoise, G. Latham, B. Larue, T. Chen, B. Isacks, J. Recy, and R. Louat (1980). Structure of the New Hebrides Arc-Trench system, *J. Geophys. Res.*, **85**, 253-266.
- Isacks, B. L., and M. Barazangi (1977). Geometry of Benioff zones: Lateral segmentation and downwards bending of the subducted lithosphere, in M. Talwani and W. C. Pitman, III, Editors, *Island Arcs, Deep Sea Trenches, and Back-Arc Basins*, Maurice Ewing Series 1, American Geophysical Union, Washington, D.C., 99-114.
- Isacks, B. L., R. K. Cardwell, J. L. Chatelain, M. Barazangi, J. M. Marthelot, D. Chinn, and R. Louat (1981). Seismicity and tectonics of the central New Hebrides Island Arc, in *Earthquake Prediction*, Maurice Ewing Series 4, D. Simpson and P. Richards, Editors, American Geophysical Union, Washington, D.C. 93-116.
- Kaila, K., and V. Krishna (1978). Upper mantle velocity structure in the New Hebrides island arc region, *J. Phys. Earth*, **26**, S139-S153.
- Karig, D. and J. Mammerickx (1972). Tectonic framework of the New Hebrides island arc, *Mar. Geol.*, **12**, 187-205.
- Maillet, P., M. Monzier, M. Selo, and D. Storzer (1982). La zone d'Entrecasteaux (sud-ouest Pacifique): nouvelle approche petrologique et geochronologique, in Equipe de Geologie-Geophysique du Centre ORSTOM de Noumea, Contribution a l'etude geodynamique du Sud-Ouest Pacifique, *Travaux et Documents de l'ORST and OM*, **147**, 441-458.
- Mallick, D. I. J., G. Neef (1974). Geology of Pentecost, New Hebrides Geological Survey Regional Report, British Residency, Vila, New Hebrides, 103 pp.
- Mammerickx, J., T. E. Chase, S. M. Smith, and I. L. Taylor (1973) Bathymetry of the South Pacific, Scripps Institution of Oceanography, La Jolla, Calif.
- Marthelot, J.-M., J.-L. Chatelain, B. L. Isacks, R. K. Cardwell, and E. Coudert (1985). Seismicity and attenuation in the central Vanuatu (New Hebrides) islands: a new interpretation of the effect of subducting the D'Entrecasteaux fracture zone, *J. Geophys. Res.*, **82**, 8641-8650.
- Mitchell, A. H. G. and A. J. Warden (1971). Geological evolution of the New Hebrides island arc, *J. Geol. Soc. London*, **127**, 501-529.
- Monzier, M., J. Y. Collot, and J. Daniel, (1984). Carte bathymetrique des parties centrale et meridionale de l'arc insulaire des Nouvelles-Hébrides, Office de la Recherche Scientifique et Technique Outre-Mer, Paris.
- National Earthquake Information Service, Preliminary Determination of Epicenters (PDE), monthly bulletin, 1981. U.S. Geological Survey, Alexandria, VA.
- Parsons, B., and J. G. Sclater (1977). An analysis of the variation of ocean floor bathymetry and heat flow with age, *J. Geophys. Res.*, **82**, 803-827.
- Pascal, G., B. L. Isacks, M. Barazangi, and J. Dubois (1978). Precise relocation of earthquakes and seismotectonics of the New Hebrides island arc, *J. Geophys. Res.*, **83**, 4958-4973.
- Paterson, M. S. (1987). Problems in the extrapolation of laboratory rheological data, *Tectonophysics*, **133**, 33-43.
- Tarantola, A. and B. Valette (1982). Inverse Problems=Quest for Information, *J. Geophys.*, **50**, 159-170.
- Weins, D. A. and S. Stein (1983). Age dependence of oceanic intraplate seismicity and implications for lithospheric evolution, *J. Geophys. Res.*, **88**, 6455-6468.
- Weins, D. A. and S. Stein (1984). Intraplate seismicity and stresses in young oceanic lithosphere, *J. Geophys. Res.*, **89**, 11442-11464.
- Weissel, J. K., A. B. Watts and A. Lapoville (1981). Magnetic anomaly evidence for late Paleocene to late Eocene seafloor in the southern New Hebrides basin, *J. Geophys. Res.*, **86**.

DEPARTMENT OF GEOLOGY
RENSSELAER POLYTECHNIC INSTITUTE
TROY, NEW YORK (S.W.R.)

INSTITUTE FOR THE STUDY OF THE CONTINENTS
CORNELL UNIVERSITY
ITHACA, NEW YORK (B.L.I.)

INSTITUT OF FRANCAIS DE RECHERCHE SCIENTIFIQUE POUR LE
DEVELOPPEMENT EN COOPERATION (ORSTOM)
NOUMEA, NEW CALEDONIA (J.-L.C.)